**Title**

Voxel-Wise Co-analysis of Macro- and Microstructural Brain Alteration in Mild Cognitive Impairment and Alzheimer's Disease Using Anatomical and Diffusion MRI

**Authors**

Cardenas, Valerie A
Tosun, Duygu
Chao, Linda L
et al.

Peer reviewed

# Voxel-wise co-analysis of macro- and microstructural brain alteration in Mild Cognitive Impairment and Alzheimer's disease using anatomical and diffusion MRI

**Valerie A. Cardenas, Ph.D.**[*,a,b], **Duygu Tosun, Ph.D.**[a,b], **Linda L. Chao, Ph.D.**[a,b], **P. Thomas Fletcher, Ph.D.**[c], **Sarang Joshi, Ph.D.**[c], **Michael W. Weiner, M.D.**[a,b], and **Norbert Schuff, Ph.D.**[a,b]

[a]University of California, San Francisco

[b]Veterans Affairs Medical Center, San Francisco

[c]University of Utah

## Abstract

**Background and Purpose**—To determine if a voxel-wise "co-analysis" of structural and diffusion tensor magnetic resonance imaging (MRI) together reveals additional brain regions affected in mild cognitive impairment (MCI) and Alzheimer's Disease (AD) than voxel-wise analysis of the individual MRI modalities alone.

**Methods**—Twenty-one patients with MCI, 21 patients with AD, and 21 cognitively normal healthy elderly were studied with MRI. Maps of deformation and fractional anisotropy (FA) were computed and used as dependent variables in univariate and multivariate statistical models.

**Results**—Univariate voxel-wise analysis of macrostructural changes in MCI showed atrophy in the right anterior temporal lobe, left posterior parietal/precuneus region, WM adjacent to the cingulate gyrus, and dorsolateral prefrontal regions, consistent with prior research. Univariate voxel-wise analysis of microstructural changes in MCI showed reduced FA in the left posterior parietal region extending into the corpus callosum, consistent with previous work. The multivariate analysis, which provides more information than univariate tests when structural and FA measures are correlated, revealed additional MCI-related changes in corpus callosum and temporal lobe.

**Conclusion**—These results suggest that in corpus callosum and temporal regions macro- and microstructural variations in MCI can be congruent, providing potentially new insight into the mechanisms of brain tissue degeneration.

### Keywords

MANOVA; deformation morphometry; fractional anisotropy; multimodality imaging; multivariate statistics; univariate statistics

Corresponding Author: Valerie A. Cardenas, University of California, San Francisco, Department of Veterans Affairs Medical Center, 4150 Clement St. (114M), San Francisco CA 94121, Tel: (415) 221-4810 x4086, Fax: (415) 668-2864, valerie.cardenas-nicolson@ieee.org.

There are no conflicts of interest to report.

## 1. Introduction

Alzheimer disease (AD) pathology is a progressive neurodegenerative condition in aging, starting typically with very mild cognitive symptoms before advancing to mild cognitive impairment (MCI) and potentially to dementia. Studies of AD, and its precursor MCI, have observed that deficits in cognition[1, 2] are correlated with regional MRI-detected macrostructural[3–5] and microstructural changes[6, 7]. Moreover, new findings from biomarker studies show that cognitive deficits in MCI can be paralleled by abnormal levels of amyloid-β (Aβ) protein in cerebrospinal fluid (CSF)[8] as well as by elevated Aβ accumulation in the brain[9, 10]. Since Aβ is one of the hallmarks of AD, these findings provide evidence for presence of AD pathology in MCI subjects. Consequently, the characteristic pattern of brain alterations in MCI seen on MRI reflects potentially AD pathology.

Conventional T1-weighted imaging is the gold standard for in-vivo assessment of brain macrostructure, i.e. the gross anatomy of the living brain, and the characteristic pattern of atrophy in patients with MCI is well described. Volumetric MRI region of interest (ROI) studies have reported atrophy of the hippocampus, entorhinal, and parahippocampal cortices of cognitively impaired but non-demented patients compared to healthy elderly[11–13]. Voxel-wise whole brain analyses in MCI patients compared to controls have reported decreased gray matter (GM) density in medial and lateral temporal, cingulate, and thalamic regions[3, 14]. In the clinically defined stages of AD, GM loss is also evident in the precuneus, frontal, and parietal regions[15]. In contrast to gray matter atrophy, measurement of regional white matter (WM) volumes using structural T1-weighted MRI is ill-defined, since WM has mostly uniform contrast and there is a lack of distinguishable anatomical boundaries. As a result, fewer studies have examined regional WM macrostructural changes, but smaller volumes of WM in MCI versus healthy elderly have been reported in the corpus callosum, cingulum bundle, and temporal and frontal lobes[16, 17]. Greater WM tissue loss over 18 months has also been shown in amnestic MCI patients compared to healthy elderly, though regions of detectable atrophy at baseline can be very small[18]. Widespread WM atrophy has been reported in patients diagnosed with AD[19–21].

There is growing evidence from diffusion tensor imaging (DTI) studies that microstructural integrity of WM can also be compromised in MCI and AD. Microstructural WM changes may include a host of alterations, including demyelination, microtubule disruption, cytoskeletal changes, membrane degradation and axonal deletion[22]. DTI affords a means of examining WM microstructure in vivo, by measuring the random mobility of tissue water thereby obtaining an imprint of the intrinsic structural consistency of white matter, such as integrity of white matter fiber bundles. In particular, fractional anisotropy (FA), which is an index of the orientation dependence of water diffusion within a voxel, is thought to provide a sensitive measure for the integrity of fiber bundles. Decreases in FA imply that the integrity of WM brain structures has been compromised, and may signify the breakdown of microstructural components. DTI studies of MCI have consistently shown reduced FA in the posterior cingulum, which is known to be connected to the hippocampus and parahippocampal regions[7, 23–25]. Other regions with reduced FA in MCI include temporal WM[26], parietal WM[24, 27], corpus callosum[16] and parahippocampal WM[7, 25], and reduced

mean diffusivity and FA in the hippocampus[28]. DTI studies in AD have generally demonstrated a similar, but more pronounced, pattern of FA abnormalities[29].

These neuroimaging results show that FA and measures of brain volume are promising potential early markers of MCI and AD, evaluated independently. The studies cited above did not compare tissue volume and FA changes on the same subjects, however, so it is unclear if there are regions of the brain where FA abnormalities occur in the absence of atrophy, or where atrophy occurs in regions of normal FA. There may also be regions of the brain where the degenerative process has started, leading to concomitant FA and tissue volume changes, but there is insufficient statistical power to detect such small changes.

The overall goal of this study was to evaluate micro-structural brain alterations and macrostructural changes in the same subjects, to determine whether FA abnormalities and atrophy co-occur in MCI and AD. We used voxel-wise analysis of structural and diffusion MRI separately, but also explored the use of a voxel-wise "co-analysis" of the two MR modalities using a multivariate analysis of variance (MANOVA) model. The probability of any Type I statistical error increases with the number of statistical tests. Most multiple correction adjustments for p-values assume independence of the tests, but since the structural and diffusion images arise from a common anatomy they are unlikely to be independent, and such adjustments would be conservative. MANOVA can exploit the cross-correlations between structural and diffusion MRI, is often more powerful than ANOVA, and there is a greater chance of detecting effects. Therefore, we hypothesized that a co-analysis of structural and diffusion tensor MRI together would enable detection of abnormalities in regions where small magnitude macro- and microstructural MCI-related WM changes were co-occurring. Specifically, we hypothesized that 1) analysis of structural MRI would reveal MCI- and AD-related atrophy primarily in the temporal lobes, posterior cingulate, and thalamus, 2) analysis of DTI would reveal MCI- and AD-related FA reductions in the posterior cingulum, and 3) co-analysis of structural and DTI in MCI patients would reveal brain abnormalities in regions that are usually not detected until patients are diagnosed with AD, such as the corpus callosum and fiber tracts connecting the hippocampal area and cingulum.

## 2. Methods

### 2.1 Participants

Participants were recruited by advertisements in the community or referred by one of several memory clinics in the San Francisco Bay Area, including the Memory Disorders Clinic at the San Francisco Veterans Affairs Medical Center, the Memory and Aging Center at the University of California, San Francisco, and the Memory Disorders Clinic at the California Pacific Medical Center, for inclusion in one of several studies. Study procedures include a neurological exam, structural MRI, diffusion MRI, and comprehensive neuropsychological testing. In compliance with the Code of Ethics of the World Medical Association and the Declaration of Helsinki, study procedures were approved by review boards of the University of California San Francisco and the San Francisco VA Medical Center, explained to all participants, written informed consent was obtained.

From the larger population studied, only participants with artifact-free structural and diffusion MRI were included. Twenty-one patients met Petersen's criteria for MCI, age: 71 ± 8 yrs, 11 women, MMSE (Mini-Mental State Examination): 29 ± 2. These patients were gender matched with 21 cognitively normal healthy elderly controls (CN), age: 70 ± 7 yrs, 11 women, MMSE 29 ± 1. The MCI patients were also gender matched with 21 patients who met AD criteria of the National Institute of Neurological and Communicative Disorders and Stroke-Alzheimer's Disease and Related Disorders Association (NINCDS/ADRDA), age: 69 ± 9, 11 women, MMSE 21 ± 7. As evidenced by the high MMSE scores, the MCI patients were in an early stage of cognitive deficits and far less impaired than the AD patients.

## 2.2 Magnetic resonance imaging (MRI) acquisition

All scans were performed on a 4 Tesla (Bruker/Siemens) MRI system with a birdcage transmit and 8 channel receive coil arranged in the same housing. The scans included T1-weighted and T2-weighted structural MRI data for measurements of brain macro-structure and diffusion tensor MRI for measurement of micro-structure. T1-weighted images were obtained with a 3D volumetric magnetization prepared rapid gradient echo (MPRAGE) sequence, TR/TE/TI=2300/3/950 ms, timing; 7° flip angle; $1.0 \times 1.0 \times 1.0$ mm$^3$ resolution; 157 continuous sagittal slices; acquisition time of 5 min. T2-weighted images were acquired with a variable flip (VFL) angle turbo spin-echo sequence with TR/TE = 4000/30 ms and with the same resolution matrix and field of view of MPRAGE. DTI was based on a dual spin-echo refocused echo-planar imaging (EPI) sequence supplemented with parallel imaging acceleration (GRAPPA) (Griswold et al., 2002) with a factor 2 to reduce susceptibility distortions. Other imaging parameters were: TR/TE=6000/77 ms; $2 \times 2$ mm$^2$ in-plane resolution; 40 continuous 3 mm slices. A reference image (no diffusion gradient b=0) and six diffusion-weighted images (b=800s/mm$^2$ along six non-collinear direction) were acquired. Four DTI scans were acquired and averaged after motion correction to boost signal-to-noise. The total acquisition time of DTI was 4 min.

## 2.3 MRI pre-processing

In-house software, based on algorithms described in the papers referenced in this section, was used for MRI pre-processing. An expectation maximization segmentation (EMS) algorithm including correction for intensity inhomogeneity[30, 31] was applied to T1 weighted MRI, separating skull, scalp, extra-cranial tissue from the rest of brain image volume. Each individual skull-stripped and bias field corrected brain image volume was affine registered to a reference brain image to adjust for global differences in brain positioning and scale across individuals. For this study, an unbiased average brain image was used as the reference. The unbiased average brain was generated from 10 healthy elderly individual brains (i.e., age of 50 to 70) that were not part of the CN group using an unbiased atlas formation technique based on large deformations mapping[32]. A large deformation diffeomorphic mapping algorithm using fluid-flow registration[33] was used to register individual scans to standard image space of the unbiased atlas brain. The Jacobian determinant of this transformation was computed at each voxel (resolution 1×1×1 mm$^3$), giving the pattern of volume change required to force the individual anatomy to conform to the reference. The Jacobian images were log transformed to achieve a more normal

distribution and then smoothed using a Gaussian filter (FWHM=10 mm) to create tissue volume maps (JAC), where the value at each voxel represents the tissue volume relative to the reference (e.g., a voxel value of 0.06 denotes a volume $vol_{ref} \times 10^{0.06}$, or about 15% greater than the reference voxel)

## 2.4 DTI pre-processing

The pre-processing pipeline aims to align a set of DTI images with the corresponding structural data through the following steps. The pre-processing pipeline used a combination of publicly available software and in-house software, based on algorithms described in the papers referenced in this section. Diffusion tensor images were corrected for eddy currents and head motion[34]. Based on a mutual information metric, the T2-weighted image was rigidly aligned to the B0 image, which is a DTI map without diffusion sensing gradients (b=0 $s/mm^2$). A variational image-based approach was used to calculate a deformation field from the B0 image to the rigidly aligned T2-weighted image to correct for susceptibility artifacts (i.e., nonlinear geometric distortion in DTI)[35]. We selected a variational approach for EPI distortion correction over the conventional field map approach, because studies have shown that the local deformations in EPI are best handled with a dense displacement field (i.e. high order deformations)[35]. In contrast, field maps can fail to completely correct geometric distortions, presumably due to limits in the physical model[36]. Concatenated eddy current transformation and the deformation field for nonlinear distortion correction were applied to all DTIs. Diffusion tensors were estimated for each subject from the diffusion tensor images using weighted least squares tensor estimation (http://teem.sourceforge.net/index.html)[37]. The T2-weighted image was rigidly aligned (http://www.fmrib.ox.ac.uk.fsl/flirt/overview.html) to the T1-weighted image and the transformation was concatenated with the inverse rigid transformation from B0 image to T2-weighted image. The resulting rigid transformation was applied to the FA image to map onto the T1-weighted structural image space of the subject. The FA image was then mapped onto the standard image space by applying the diffeomorphic mapping estimated in MRI pre-processing. FA images were then smoothed using a Gaussian filter (FWHM=10 mm) in the standard image space.

## 2.5 Statistical analyses

Statistical analyses using valmap (http://www.nitrc.org/valmap) were applied to locate voxels within the maps where MRI measures (JAC or FA) were associated with group membership (MCI vs. CN or AD vs. CN). Several linear models were fit: (1) univariate analysis with FA maps as dependent variables (DV) with group and age as independent variables (IV), (2) univariate analysis with JAC maps as DVs with group and age as IVs, and (3) multivariate analysis with joint JAC and FA maps as DVs, to assess the effects of IVs group and age on the JAC and FA together. The multivariate analysis of variance (MANOVA) analysis takes into account the covariance between JAC and FA when calculating the significance of the IV effects, and thus may be more powerful than performing independent univariate analyses if JAC and FA are correlated. Separate analyses comparing MCI to CN and AD to CN were conducted. Clusters above a p=0.005 threshold were identified in the statistical maps, and permutation testing on cluster size was used to correct for multiple comparisons[38]. Significance level was set to α=0.05 for multivariate

analysis. A Bonferroni correction was used for the univariate analyses to account for the examination of two modalities, so α=0.05/2=0.025.

## 3. Results

### 3.1 Correlations between MRI measures

Figure 1 shows the correlation between the volumetric and FA measures, computed across MCI and CN participants (left) and AD and CN participants (right). Negative and positive correlations are both observed, ranging from neglible to strong (top end of the color scale is r=|0.8|). This figure demonstrates that the volumetric and FA measures covary, supporting the use of a MANOVA model.

### 3.1 MCI vs. CN

Table 1 summarizes regions of the brain significantly associated with MCI. The top panel of Figure 2 shows analyses (1) and (2), t-statistic maps of voxels significantly related to MCI, after cluster correction for multiple comparisons. The left image shows that MCI patients have atrophy in the temporal lobe and cingulate gyrus, especially posteriorly. Multiple comparison corrected cluster analysis revealed a cluster of voxels with smaller tissue volume extending throughout the cingulate gyrus, superior longitudinal fasciculus, and extending into the dorsolateral prefrontal cortex on the right (cluster volume 27.8 cc, 14.9% smaller volume), a cluster in the right anterior temporal lobe (20.2 cc, 18.3% smaller), and a cluster in the left posterior parietal/precuneus WM (11.8 cc, 15.1% smaller).

The regions of reduced FA in the MCI patients compared to the controls encompassed a smaller volume of the brain. The top right image shows that MCI patients have reduced FA compared to CN in the posterior parietal WM/posterior corpus callosal region (cluster volume 8.1 cc, 3.8% smaller FA). Another cluster of voxels was observed in the occipital WM and GM (4.7 cc, 4.8% smaller, not shown). Since FA is not a very sensitive measure for GM alterations, it is likely that this reflects FA reductions in the WM that artifactually extends into the GM because of the 10 mm FWHM Gaussian filter that was applied to our FA maps.

The bottom panel of Figure 2 shows results from MANOVA analysis (3), which are t-statistic maps showing regions where MCI affected both JAC and FA considered jointly. The right anterior temporal was still significantly related to MCI diagnosis in the MANOVA analysis. In the multivariate analysis, the left posterior parietal/corpus callosum region previously detected using univariate analysis extended to affect the right side as well (11.9 cc, 13.6% smaller volume, 3.0% smaller FA). In addition, MCI was found to be significantly associated to JAC and FA jointly in several more brain regions. These include left anterior temporal lobe (3.5 cc, 12.8% smaller volume, 0.9% FA change), left superior frontal WM (3.0 cc, 15.9% smaller volume, 1.2% smaller FA), and brainstem (2.0 cc, 3.7% smaller volume, 6.2% smaller FA).

Figure 4 (left) overlays the significant regions detected in each analysis (MCI vs. CN). Red voxels denote significant regions from the JAC-only analysis, blue voxels from the FA-only analysis, and green from the multivariate analysis. Yellow and cyan are regions where

significance was found in both univariate and multivariate analyses. Figure 3 shows regions of green in the posterior region of the right corpus callosum and the left anterior temporal lobe, where the multivariate analysis was more sensitive to the effects of MCI on the brain than either univariate analysis.

### 3.2 AD vs. CN

Table 2 summarizes regions of the brain significantly associated with AD. The top panel of Figure 3 shows analyses (1) and (2), t-statistic maps of voxels significantly related to AD, after cluster correction for multiple comparisons. The left image shows that AD patients have atrophy in a single, very large connected cluster that includes bilateral anterior and medial temporal lobes (including entorhinal cortex and hippocampus), cingulate gyrus, corpus callosum, frontal WM, and posterior parietal/precuneus regions (cluster volume 268.2 cc, 19.0% smaller volume). In addition, a significant increase in ventricular volume is seen in AD (54.2 cc, 50.3% larger volume).

A much smaller volume of the brain showed reduced FA in the AD patients compared to the controls. The top right image shows that AD patients have reduced FA in the posterior parietal WM/posterior corpus callosal region on the right (cluster volume 15.3 cc, 5.5% smaller FA) and left (10.9 cc, 4.7% smaller).

The bottom panel of Figure 3 shows results from MANOVA analysis (3), which are t-statistic maps showing regions where AD affected both JAC and FA considered jointly. AD is jointly related to a single, very large connected cluster that is largely overlapping with the cluster detected in the univariate DBM analysis and includes bilateral anterior and medial temporal lobes (including entorhinal cortex and hippocampus), cingulate gyrus, corpus callosum, frontal WM, and posterior parietal/precuneus regions (250.4 cc, 8.3% smaller volume, 1.6% smaller FA). Multivariate analysis did not reveal any additional brain regions affected by AD.

Figure 4 (right) overlays the significant regions detected in each AD vs. CN analysis, using the color map described earlier. The regions of green shown in Figure 3 are merely slight spatial extensions of regions detected in the univariate analysis, and do not reveal new regions affected by AD.

## 4. Discussion

Univariate voxel-wise analysis of macrostructural changes in MCI showed atrophy in the right anterior temporal lobe, left posterior parietal/precuneus region, WM adjacent to the cingulate gyrus, and dorsolateral prefrontal regions. Our results are consistent with the many studies showing temporal lobe, posterior parietal/precuneus, and cingulate gyrus abnormalities in MCI[11, 39, 40]. Dorsolateral prefrontal atrophy was not hypothesized, but is consistent with a recent report of thinning in the dorsolateral prefrontal cortex of MCI patients with low executive functioning[41]. Univariate voxel-wise analysis of microstructural changes in MCI showed reduced FA in the left posterior parietal region extending into the corpus callosum, consistent with previous work[16] However, inconsistent with our predictions, FA changes in the posterior cingulum were not significant. It is possible that in

these early MCI patients FA changes have not yet occurred and/or the heterogeneity of the MCI population may have diminished systematic FA alterations in this brain region, though technical limitations, such as inaccuracies in image registration and low diffusion sensitivity because only six diffusion directions were employed at a relatively low b=800s/mm$^2$, also cannot be ruled out.

As hypothesized, the multivariate analysis, which provides theoretically more information than univariate tests when structural and DTI MRI measures are correlated, reveals additional changes in MCI. This is illustrated by the extensive regions in corpus callosum and temporal lobe, (colored green in Figure 3), that were significant in the multivariate but not univariate analyses. In particular, the finding suggests that in temporal, posterior parietal, and corpus callosum regions, structural changes are not the only manifestation of brain alterations in MCI, but are accompanied by corresponding microstructural FA changes. Moreover, the findings imply that regional macro- and microstructural variations in MCI can be congruent, providing potentially new insight into the mechanisms of brain tissue degeneration. It is noteworthy that in the right and left anterior temporal clusters found in the multivariate analysis of MCI, there was no decrease in the median FA values compared to CN. This implies that correlation between the structural and DTI measures was high, i.e. the subjects that did show reduced FA in these regions also showed the smallest volumes, so that a group difference was detected even though the FA changes in the MCI group as a whole were not apparent.

Univariate voxel-wise analysis of macrostructural changes in AD showed atrophy in most regions of the brain. There was extensive atrophy in the anterior and medial temporal lobes, frontal lobes, and posterior parietal/posterior cingulate/precuneus regions, accompanied by ventricular enlargement. It is generally accepted that these regions are affected in AD. The posterior temporal and occipital regions were largely spared. Univariate voxel-wise analysis of microstructural changes in AD showed reduced FA in the bilateral parietal WM extending into the corpus callosum. This pattern was very similar to that observed in our MCI patients, but more extensive. Macrostructural and microstructural changes co-occurred in posterior parietal and corpus callosum regions.

In contrast to the MCI vs. CN comparison, multivariate analysis did not reveal any new brain regions associated with the diagnosis of AD. There are several interpretations for this result. First, it is possible that atrophy progresses in MCI while FA measures of demyelination reach a floor, with the result that measures of macrostructure and microstructure become less correlated in AD compared to MCI. If so, separate analyses of each provide similar information, reducing the benefit of evaluating them together. It is also possible that the mechanisms underlying the DTI alterations in AD are different from those in our sample of MCI subjects, some of whom may remain stable and not convert to AD. Aside from biological variations, the findings might also be related to technical limitations. For example, the sensitivity of DTI to detect diffusion anisotropy may decline in presence of substantial atrophy as micro-structural variations happen on an increasingly finer scale. DTI studies using more powerful diffusion gradients should improve sensitivity to diffusion on a smaller microstructural scale. Another technical consideration is that FA changes, which reflect only directional variations in diffusion, may not be sensitive to other diffusion

properties, such as anomalous effects (e.g. kurtosis), which might become more important with increasing tissue loss. Lastly, it is possible that we lacked power with this small sample to detect new regions associated with AD.

It is important to understand that in the univariate model, we are assessing whether the means of each FA or deformation for patient vs. CN are taken from the same sampling distribution. Statistics (such as an F-statistic) are assessed by comparing the within and between group variances of FA or deformation. In the multivariate model, in contrast, we are testing whether the vectors (FA and deformation) of means are sampled from the same distribution. MANOVA gives a measure of the overall likelihood of that the mean vector of FA and deformation from the disease group and the mean vector for the CN group come from the same distribution. Statistics (such as Wilk's lambda) are assessed by comparing the within and between group variances *and covariances* of FA and deformation. Critical values for the F-statistic or Wilk's lambda at a desired level of α are determined, and p-values for the univariate or multivariate model interpreted as usual. As such, the p-values for the univariate and multivariate models can be directly compared. For example, if the p-value for a callosal voxel was 0.20 for the univariate FA analysis comparing MCI and CN, there is a 20% chance of observing such a test statistic computed on FA in the absence of a group difference. Similarly, if the p-value for that same voxel was 0.05 for the multivariate analysis comparing MCI and CN, there is a 5% chance of observing such a test statistic computed on FA *and* deformation in the absence of a group difference. If the confidence level is α=0.05, then the voxel would be significantly associated with the group effect in the multivariate analysis but not in the univariate analysis, and we would not need to test whether a p-value of 0.20 is significantly different from a p-value of 0.05. Intuitively, it is similar to the idea that the disease group and CN might be more easily separated in a two-dimensional feature space of FA and deformation, than when considering FA or deformation alone.

This study was limited by the small number of participants in each group. Although our group has studied many MCI, AD, and healthy elderly, we took care to only include participants with artifact-free DTI and T1-weighted imaging, and this severely impacted our sample. All MCI participants with artifact-free DTI and T1-weighted imaging were included, and the AD and healthy elderly patients were age and gender matched. In our experience, patients with better quality imaging are less impaired (i.e., better able to follow directions and lie still in the magnet). As a result, the brains in our MCI and AD samples may be more similar to our healthy elderly sample than would be generally observed. Furthermore, the characterization of the group was based exclusively on clinical symptoms and not on autopsy or CSF or PIB-PET markers. Thus, the variations in atrophy and DTI may not be related to AD pathology, and it is possible that some of the MCI-related differences are due to some other dementia etiology. Another point to consider is that a recent meta-analysis suggests that mean diffusivity is a more sensitive marker of MCI than FA[42], and it is possible that a co-analysis of atrophy and mean diffusivity would provide even more added value than our co-analysis of atrophy and FA.

Another limitation is that the T1-weighted images were used to normalize DTI to the atlas space, which may cause misregistration of white matter fibers, especially in brains with

substantial atrophy. To some degree this problem is mitigated by our use of an elderly atlas, use of a large deformation diffeomorphic mapping technique, and spatial filtering of the resulting FA maps. Although spatial filtering of the FA maps can cause partial voluming of adjacent white matter bundles which would complicate analyses such as tract tracing, in our application it can actually reduce the problems associated with misregistration. The JAC maps reflect volume of GM, WM, and CSF, while the FA maps reflect WM microstructure and provide little or no information in the GM and CSF. In this study, we did not use a simplified model excluding FA for GM and CSF voxels, but this could be implemented in future work.

In conclusion, we found that co-analysis of macrostructure (T1-weighted images) and microstructure (DTI) improved detection of brain alterations in MCI, indicating that macrostructural and microstructural alterations can be correlated and co-occur spatially, and measurement of both provides added value. However, our results also suggest that by the time patients are diagnosed with AD, the most prominent features of brain alterations on MRI are macrostructural changes while the value of measuring concurrent microstructural changes is diminished. The multivariate approach may be extended to co-analysis of individual structural and DTI MRI for improved detection and staging of early brain alterations related to cognitive deficits which might lead to AD.

## Acknowledgments

## References

1. Iachini I, Iavarone A, Senese VP, Ruotolo F, Ruggiero G. Visuospatial memory in healthy elderly, AD and MCI: a review. Curr Aging Sci. 2009; 2:43–59. [PubMed: 20021398]

2. Taler V, Phillips NA. Language performance in Alzheimer's disease and mild cognitive impairment: a comparative review. J Clin Exp Neuropsychol. 2008; 30:501–556. [PubMed: 18569251]

3. Karas GB, Scheltens P, Rombouts SA, Visser PJ, van Schijndel RA, Fox NC, Barkhof F. Global and local gray matter loss in mild cognitive impairment and Alzheimer's disease. Neuroimage. 2004; 23:708–716. [PubMed: 15488420]

4. Apostolova LG, Thompson PM. Mapping progressive brain structural changes in early Alzheimer's disease and mild cognitive impairment. Neuropsychologia. 2008; 46:1597–1612. [PubMed: 18395760]

5. Mueller SG, Schuff N, Yaffe K, Madison C, Miller B, Weiner MW. Hippocampal atrophy patterns in mild cognitive impairment and Alzheimer's disease. Hum Brain Mapp. 2010; 31:1339–1347. [PubMed: 20839293]

6. Liu Y, Spulber G, Lehtimaki KK, Kononen M, Hallikainen I, Grohn H, Kivipelto M, Hallikainen M, Vanninen R, Soininen H. Diffusion tensor imaging and Tract-Based Spatial Statistics in Alzheimer's disease and mild cognitive impairment. Neurobiol Aging. 2011; 32:1558–1571. [PubMed: 19913331]

7. Zhang Y, Schuff N, Jahng GH, Bayne W, Mori S, Schad L, Mueller S, Du AT, Kramer JH, Yaffe K, Chui H, Jagust WJ, Miller BL, Weiner MW. Diffusion tensor imaging of cingulum fibers in mild cognitive impairment and Alzheimer disease. Neurology. 2007; 68:13–19. [PubMed: 17200485]

8. Okonkwo OC, Mielke MM, Griffith HR, Moghekar AR, O'Brien RJ, Shaw LM, Trojanowski JQ, Albert MS. Cerebrospinal fluid profiles and prospective course and outcome in patients with amnestic mild cognitive impairment. Arch Neurol. 68:113–119. [PubMed: 21220682]

9. Villemagne VL, Pike KE, Chetelat G, Ellis KA, Mulligan RS, Bourgeat P, Ackermann U, Jones G, Szoeke C, Salvado O, Martins R, O'Keefe G, Mathis CA, Klunk WE, Ames D, Masters CL, Rowe CC. Longitudinal assessment of Abeta and cognition in aging and Alzheimer disease. Ann Neurol. 69:181–192. [PubMed: 21280088]

10. Tolboom N, van der Flier WM, Yaqub M, Koene T, Boellaard R, Windhorst AD, Scheltens P, Lammertsma AA, van Berckel BN. Differential association of [11C]PIB and [18F]FDDNP binding with cognitive impairment. Neurology. 2009; 73:2079–2085. [PubMed: 20018636]

11. Jack CR, Petersen RC, Xu YC, O'Brien PC, Smith GE, Ivnik RJ, Boeve BF, Waring SC, Tangalos EG, Kokmen E. Prediction of AD with MRI-based hippocampal volume in mild cognitive impairment. Neurology. 1999; 52:1397–1403. [PubMed: 10227624]

12. Du AT, Schuff N, Amend D, Laakso MP, Hsu YY, Jagust WJ, Yaffe K, Kramer JH, Reed B, Norman D, Chui HC, Weiner MW. Magnetic resonance imaging of the entorhinal cortex and hippocampus in mild cognitive impairment and Alzheimer's disease. J Neurol Neurosurg Psychiatry. 2001; 71:441–447. [PubMed: 11561025]

13. Killiany RJ, Hyman BT, Gomez-Isla T, Moss MB, Kikinis R, Jolesz F, Tanzi R, Jones K, Albert MS. MRI measures of entorhinal cortex vs hippocampus in preclinical AD. Neurology. 2002; 58:1188–1196. [PubMed: 11971085]

14. Chetelat G, Landeau B, Eustache F, Mezenge F, Viader F, de la Sayette V, Desgranges B, Baron JC. Using voxel-based morphometry to map the structural changes associated with rapid conversion in MCI: a longitudinal MRI study. Neuroimage. 2005; 27:934–946. [PubMed: 15979341]

15. Thompson PM, Hayashi KM, de Zubicaray G, Janke AL, Rose SE, Semple J, Herman D, Hong MS, Dittmer SS, Doddrell DM, Toga AW. Dynamics of gray matter loss in Alzheimer's disease. J Neurosci. 2003; 23:994–1005. [PubMed: 12574429]

16. Di Paola M, Di Iulio F, Cherubini A, Blundo C, Casini AR, Sancesario G, Passafiume D, Caltagirone C, Spalletta G. When, where, and how the corpus callosum changes in MCI and AD: a multimodal MRI study. Neurology. 2010; 74:1136–1142. [PubMed: 20368633]

17. Fan Y, Batmanghelich N, Clark CM, Davatzikos C. Spatial patterns of brain atrophy in MCI patients, identified via high-dimensional pattern classification, predict subsequent cognitive decline. Neuroimage. 2008; 39:1731–1743. [PubMed: 18053747]

18. Villain N, Fouquet M, Baron JC, Mezenge F, Landeau B, de La Sayette V, Viader F, Eustache F, Desgranges B, Chetelat G. Sequential relationships between grey matter and white matter atrophy and brain metabolic abnormalities in early Alzheimer's disease. Brain. 2010; 133:3301–3314. [PubMed: 20688814]

19. Teipel SJ, Hampel H, Alexander GE, Schapiro MB, Horwitz B, Teichberg D, Daley E, Hippius H, Moller HJ, Rapoport SI. Dissociation between corpus callosum atrophy and white matter pathology in Alzheimer's disease. Neurology. 1998; 51:1381–1385. [PubMed: 9818864]

20. Li S, Pu F, Shi F, Xie S, Wang Y, Jiang T. Regional white matter decreases in Alzheimer's disease using optimized voxel-based morphometry. Acta Radiol. 2008; 49:84–90. [PubMed: 18210317]

21. Yoon B, Shim YS, Hong YJ, Koo BB, Kim YD, Lee KO, Yang DW. Comparison of diffusion tensor imaging and voxel-based morphometry to detect white matter damage in Alzheimer's disease. J Neurol Sci. 2011; 302:89–95. [PubMed: 21168157]

22. Moseley M. Diffusion tensor imaging and aging - a review. NMR Biomed. 2002; 15:553–560. [PubMed: 12489101]

23. Fellgiebel A, Muller MJ, Wille P, Dellani PR, Scheurich A, Schmidt LG, Stoeter P. Color-coded diffusion-tensor-imaging of posterior cingulate fiber tracts in mild cognitive impairment. Neurobiol Aging. 2005; 26:1193–1198. [PubMed: 15917103]

24. Medina D, DeToledo-Morrell L, Urresta F, Gabrieli JD, Moseley M, Fleischman D, Bennett DA, Leurgans S, Turner DA, Stebbins GT. White matter changes in mild cognitive impairment and AD: A diffusion tensor imaging study. Neurobiol Aging. 2006; 27:663–672. [PubMed: 16005548]

25. Rose SE, McMahon KL, Janke AL, O'Dowd B, de Zubicaray G, Strudwick MW, Chalk JB. Diffusion indices on magnetic resonance imaging and neuropsychological performance in amnestic mild cognitive impairment. J Neurol Neurosurg Psychiatry. 2006; 77:1122–1128. [PubMed: 16754694]

26. Fellgiebel A, Wille P, Muller MJ, Winterer G, Scheurich A, Vucurevic G, Schmidt LG, Stoeter P. Ultrastructural hippocampal and white matter alterations in mild cognitive impairment: a diffusion tensor imaging study. Dement Geriatr Cogn Disord. 2004; 18:101–108. [PubMed: 15087585]

27. Stahl R, Dietrich O, Teipel SJ, Hampel H, Reiser MF, Schoenberg SO. White matter damage in Alzheimer disease and mild cognitive impairment: assessment with diffusion-tensor MR imaging and parallel imaging techniques. Radiology. 2007; 243:483–492. [PubMed: 17456872]

28. Muller MJ, Greverus D, Weibrich C, Dellani PR, Scheurich A, Stoeter P, Fellgiebel A. Diagnostic utility of hippocampal size and mean diffusivity in amnestic MCI. Neurobiol Aging. 2007; 28:398–403. [PubMed: 16529847]

29. Mueller S, Keeser D, Reiser MF, Teipel S, Meindl T. Functional and Structural MR Imaging in Neuropsychiatric Disorders, Part 1: Imaging Techniques and Their Application in Mild Cognitive Impairment and Alzheimer Disease. AJNR Am J Neuroradiol. 2011 Dec 15. [Epub ahead of print].

30. Van Leemput K, Maes F, Vandermeulen D, Suetens P. Automated model-based tissue classification of MR images of the brain. IEEE Trans Med Imaging. 1999; 18:897–908. [PubMed: 10628949]

31. Van Leemput K, Maes F, Vandermeulen D, Suetens P. Automated model-based bias field correction of MR images of the brain. IEEE Trans Med Imaging. 1999; 18:885–896. [PubMed: 10628948]

32. Lorenzen P, Davis B, Joshi S. Unbiased atlas formation via large deformations metric mapping. Med Image Comput Comput Assist Interv. 2005; 8:411–418. [PubMed: 16685986]

33. Joshi S, Davis B, Jomier M, Gerig G. Unbiased diffeomorphic atlas construction for computational anatomy. Neuroimage. 2004; 23(Suppl 1):S151–S160. [PubMed: 15501084]

34. Rohde GK, Barnett AS, Basser PJ, Marenco S, Pierpaoli C. Comprehensive approach for correction of motion and distortion in diffusion-weighted MRI. Magn Reson Med. 2004; 51:103–114. [PubMed: 14705050]

35. Tao, R.; Fletcher, PT.; Gerber, S.; Whitaker, RT. A variational image-based approach to the correction of susceptibility artifacts in the alignment of diffusion weighted and structural MRI. In: Prince, JL.; Pham, DL.; Myers, KJ., editors. IPMI. Berlin Heidelberg: Springer-Verlag; 2009. p. 664-675.

36. Wu M, Chang LC, Walker L, Lemaitre H, Barnett AS, Marenco S, Pierpaoli C. Comparison of EPI distortion correction methods in diffusion tensor MRI using a novel framework. Med Image Comput Comput Assist Interv. 2008; 11:321–329. [PubMed: 18982621]

37. Salvador R, Pena A, Menon DK, Carpenter TA, Pickard JD, Bullmore ET. Formal characterization and extension of the linearized diffusion tensor model. Hum Brain Mapp. 2005; 24:144–155. [PubMed: 15468122]

38. Nichols TE, Holmes AP. Nonparametric permutation tests for functional neuroimaging: a primer with examples. Hum Brain Mapp. 2002; 15:1–25. [PubMed: 11747097]

39. Choo IH, Lee DY, Oh JS, Lee JS, Lee DS, Song IC, Youn JC, Kim SG, Kim KW, Jhoo JH, Woo JI. Posterior cingulate cortex atrophy and regional cingulum disruption in mild cognitive impairment and Alzheimer's disease. Neurobiol Aging. 2010; 31:772–779. [PubMed: 18687503]

40. Apostolova LG, Steiner CA, Akopyan GG, Dutton RA, Hayashi KM, Toga AW, Cummings JL, Thompson PM. Three-dimensional gray matter atrophy mapping in mild cognitive impairment and mild Alzheimer disease. Arch Neurol. 2007; 64:1489–1495. [PubMed: 17923632]

41. Chang YL, Jacobson MW, Fennema-Notestine C, Hagler DJ Jr, Jennings RG, Dale AM, McEvoy LK. Level of executive function influences verbal memory in amnestic mild cognitive impairment and predicts prefrontal and posterior cingulate thickness. Cereb Cortex. 2010; 20:1305–1313. [PubMed: 19776343]

42. Clerx L, Visser PJ, Verhey F, Aalten P. New MRI markers for Alzheimer's disease: a meta-analysis of diffusion tensor imaging and a comparison with medial temporal lobe measurements. J Alzheimers Dis. 2012; 29:405–429. [PubMed: 22330833]
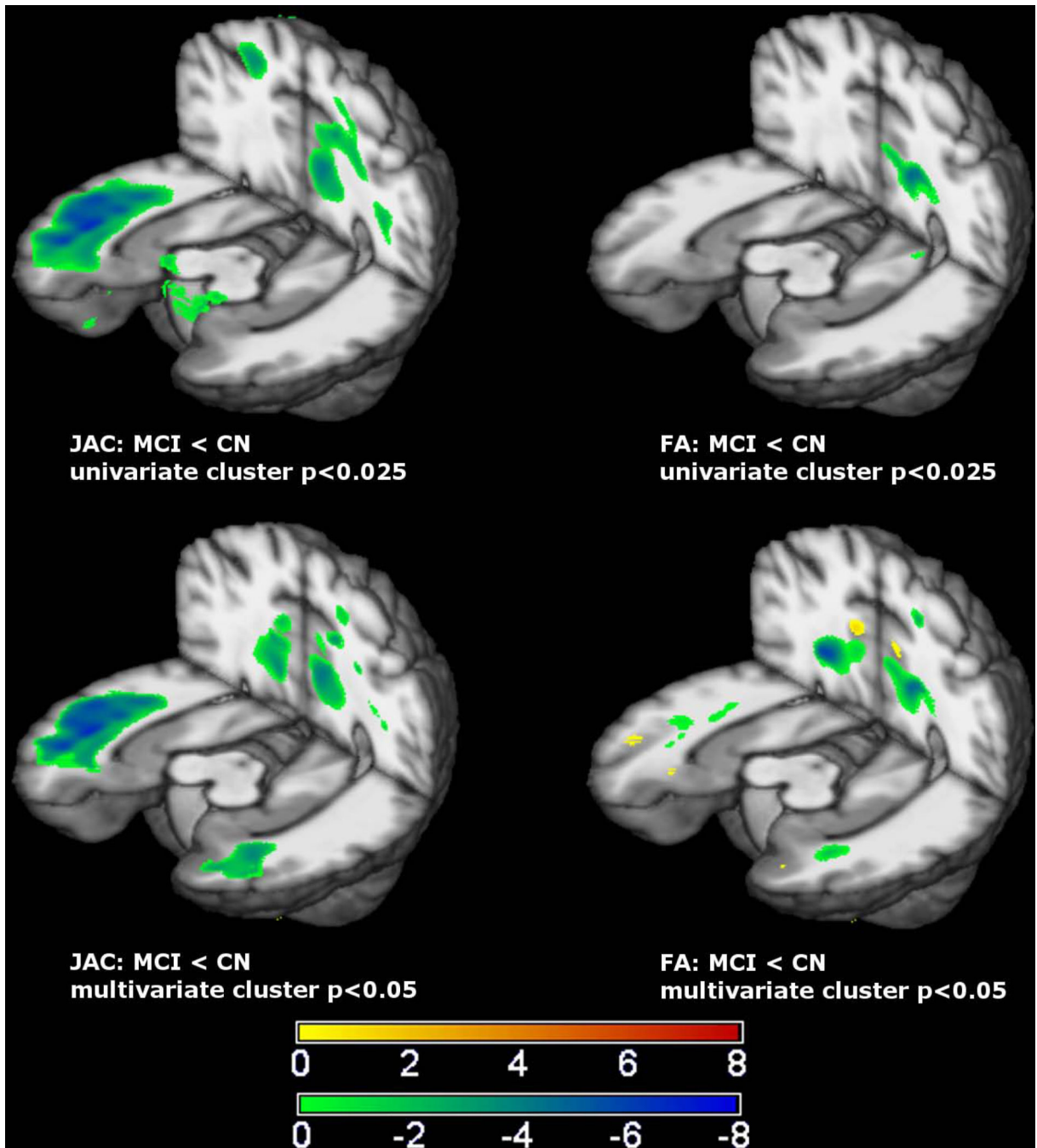
**Figure 1.**
Correlation between log10 Jacobian and FA measures across CN and MCI participants (left) and CN and AD participants (right). Negative correlations are shown in green-blue, and positive correlations in yellow-red.
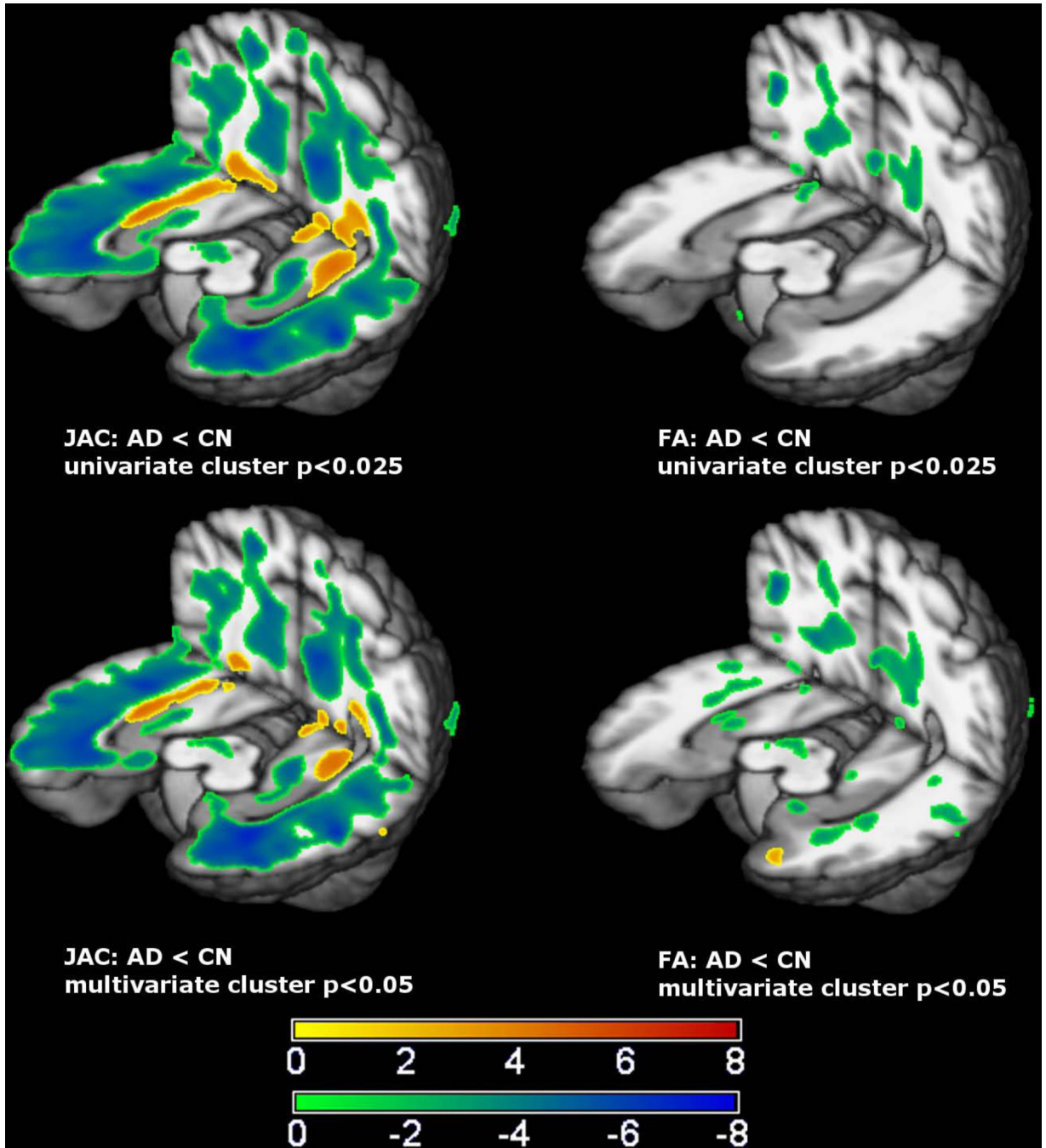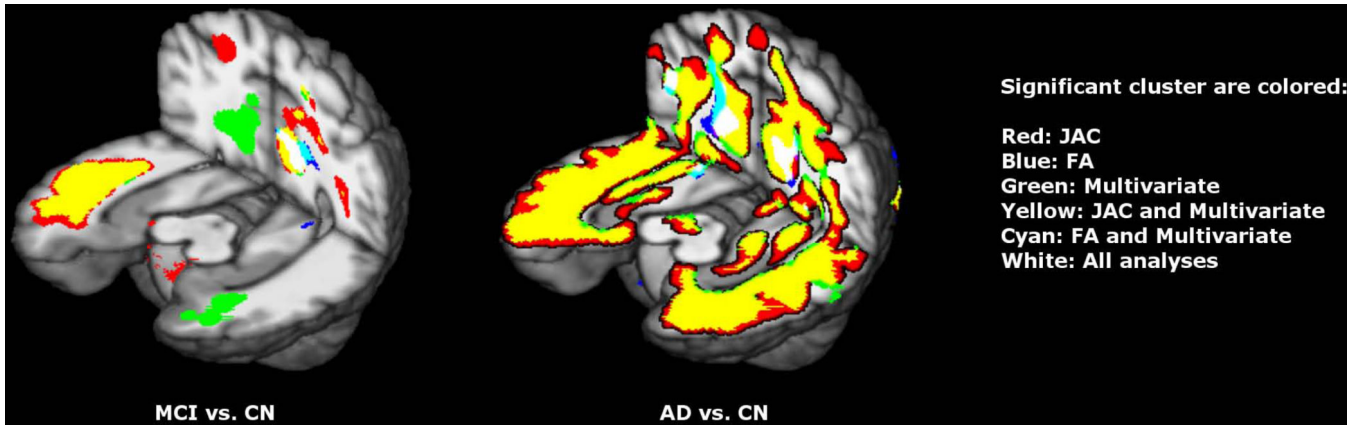
**Figure 2.**
The T-statistics for the group effect within significant clusters, after cluster correction for multiple comparisons, are shown overlaid on the atlas brain. The green-blue color scale shows regions of smaller volume (JAC-Jacobian) or lower fractional anisotropy (FA) in patients with mild cognitive impairment (MCI) versus cognitively normal (CN) elderly, and the yellow-red scale shows larger volume or higher FA. The top panel shows MCI-related differences from univariate analyses (either the Jacobian-JAC or FA maps were dependent

variables), and the bottom panel shows MCI-related differences from multivariate analysis (JAC and FA joint dependent variables).

**Figure 3.**
The T-statistics for the group effect within significant clusters, after cluster correction for multiple comparisons, are shown overlaid on the atlas brain. The green-blue color scale shows regions of smaller volume (JAC-Jacobian) or lower fractional anisotropy (FA) in patients with mild Alzheimer's disease (AD) versus cognitively normal (CN) elderly, and the yellow-red scale shows larger volume or higher FA. The top panel shows AD-related differences from univariate analyses (either the Jacobian-JAC or FA maps were dependent variables), and the bottom panel shows MCI-related differences from multivariate analysis (JAC and FA joint dependent variables).
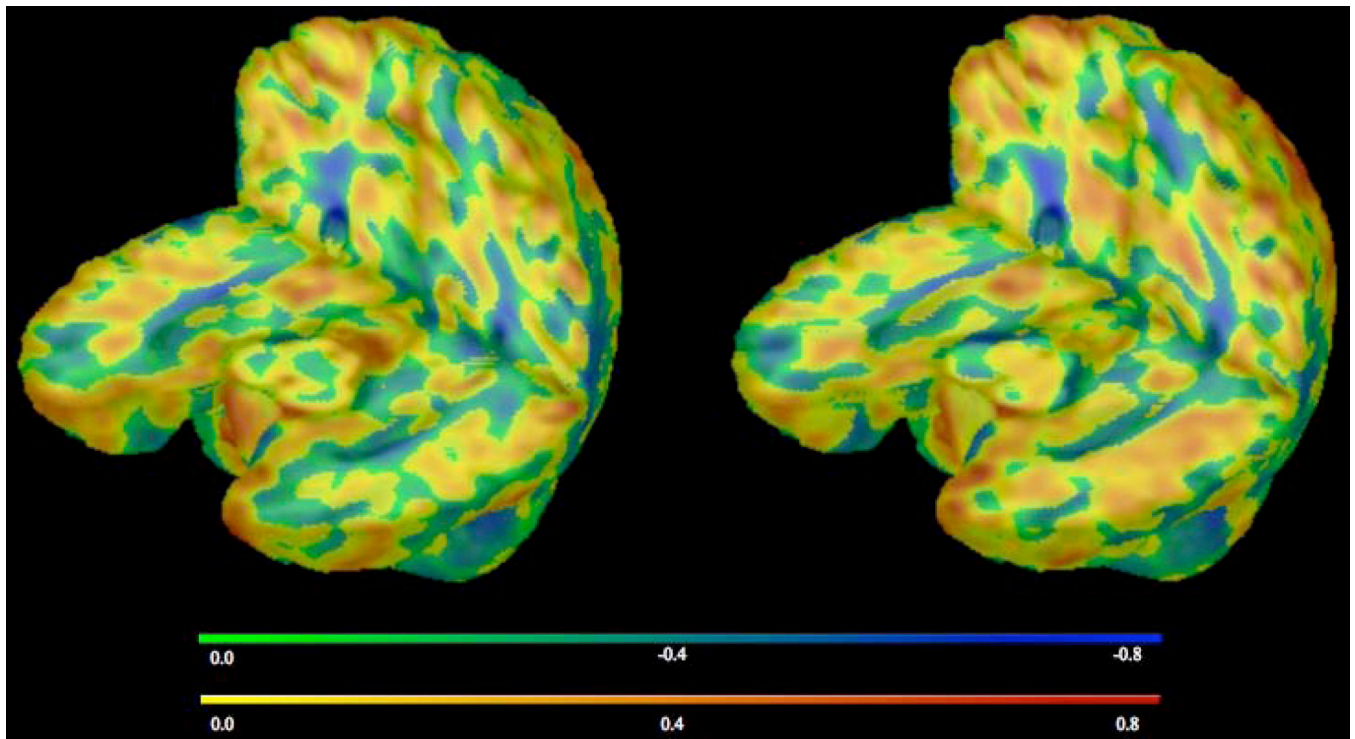
**Figure 4.**
The overlay of significant clusters of abnormal brain volume (JAC), fractional anisotropy (FA), or both (multivariate) related to mild cognitive impairment (MCI) or Alzheimer's disease (AD) are shown. Regions where group differences were observed when the dependent variables were JAC maps are colored red, when dependent variables were FA maps are colored blue, and when dependent variables were JAC and FA considered jointly (multivariate) are colored green. Regions where group differences were observed in both univariate JAC and multivariate analyses are colored yellow, in both univariate FA and multivariate analyses are colored cyan, and in all analyses are colored white.

**Table 1**

MCI vs. CN, regions with significant volume (JAC) or FA differences.

| Analysis | Location of region | Cluster Volume (cc) | Median log$_{10}$ JAC CN | Median log$_{10}$ JAC MCI | Median FA CN | Median FA MCI |
|---|---|---|---|---|---|---|
| Univariate JAC | Right frontal WM near anterior cingulate, dorso-lateral prefrontal cortex | 27.9 | −0.075 | −0.151 | NA | NA |
| | Right anterior temporal lobe | 20.2 | −0.028 | −0.114 | NA | NA |
| | Left posterior parietal/precuneus | 11.8 | −0.069 | −0.136 | NA | NA |
| Univariate FA | Bilateral occipital lobe | 8.1 | NA | NA | 0.178 | 0.137 |
| | Left posterior parietal/posterior corpus callosum | 4.7 | NA | NA | 0.323 | 0.280 |
| Multivariate, JAC and FA considered jointly | Right anterior temporal lobe | 28.6 | −0.039 | −0.086 | 0.238 | 0.238 |
| | Bilateral posterior parietal/posterior corpus callosum | 11.9 | −0.052 | −0.115 | 0.348 | 0.321 |
| | Left anterior temporal lobe | 3.5 | −0.055 | −0.106 | 0.225 | 0.240 |
| | Left superior frontal white matter | 3.0 | −0.056 | −0.142 | 0.268 | 0.251 |
| | Brainstem | 2.0 | 0.001 | −0.004 | 0.297 | 0.236 |

*
negative numbers indicate % smaller JAC or FA in MCI vs. healthy elderly CN

25

**Table 2**

AD vs. CN, regions with significant volume (JAC) or FA differences.

| Analysis | Location of region | Cluster Volume (cc) | Median log$_{10}$ JAC CN | Median log$_{10}$ JAC MCI | Median FA CN | Median FA MCI |
|---|---|---|---|---|---|---|
| Univariate JAC | Bilateral anterior and medial temporal lobes (including entorhinal cortex and hippocampus), cingulate gyrus, corpus callosum, frontal WM, posterior parietal/precuneus | 268.3 | −0.050 | −0.146 | NA | NA |
| | Bilateral ventricles | 54.2 | −0.097 | 0.063 | NA | NA |
| Univariate FA | Right lateral posterior parietal/posterior corpus callosum | 15.3 | NA | NA | 0.318 | 0.262 |
| | Bilateral ventricles, left posterior corpus callosum | 10.9 | NA | NA | 0.276 | 0.231 |
| Multivariate, JAC and FA considered jointly | Bilateral anterior and medial temporal lobes (including entorhinal cortex and hippocampus), cingulate gyrus, corpus callosum, frontal WM, posterior parietal/precuneus | 250.3 | −0.072 | −0.105 | 0.290 | 0.279 |

*
negative numbers indicate % smaller JAC or FA in AD vs. healthy elderly CN